Proc. Natl. Acad. Sci. USA
Vol. 91, pp. 33–37, January 1994
Biophysics

Quantitative magnetic resonance imaging of human brain perfusion at 1.5 T using steady-state inversion of arterial water

(cerebral blood flow/functional imaging/adiabatic fast passage/nuclear magnetic resonance *in vivo*)

DAVID A. ROBERTS*†, JOHN A. DETRE‡, LIZANN BOLINGER*, ERIK K. INSKO*, AND JOHN S. LEIGH, JR.*

Departments of *Radiology and ‡Neurology, University of Pennsylvania, Philadelphia, PA 19104

Communicated by Mildred Cohn, September 16, 1993

ABSTRACT **We report our experience using a noninvasive magnetic resonance technique for quantitative imaging of human brain perfusion at 1.5 T. This technique uses magnetically inverted arterial water as a freely diffusible blood flow tracer. A perfusion image is calculated from magnetic resonance images acquired with and without arterial blood inversion and from an image of the apparent spin-lattice relaxation time. Single-slice perfusion maps were obtained from nine volunteers with approximately 1 × 2 × 5-mm resolution in an acquisition time of 15 min. Analysis yielded average perfusion rates of 93 ± 16 ml·100 g^{-1}·min^{-1} for gray matter, 38 ± 10 ml·100 g^{-1}·min^{-1} for white matter, and 52 ± 8 ml·100 g^{-1}·min^{-1} for whole brain. Significant changes in perfusion were observed during hyperventilation and breath holding. This technique may be used for quantitative measurement of perfusion in human brain without the risks and expense of methods which use exogenous tracers.**

Tissue-specific cerebral blood flow (perfusion) is altered in many diseases, including stroke, epilepsy, and neoplasia, as well as in functional activation of normal brain. The ability to measure perfusion is useful in the diagnosis and management of these diseases and provides a valuable research tool for the study of cognitive function. Existing methods for perfusion imaging involve either injection or inhalation of an exogenous tracer compound. Such compounds include $H_2{}^{15}O$ in positron emission tomography (1, 2), xenon in computed tomography (3), and gadolinium chelates (4, 5), deuterium (6, 7), and fluorocarbons (8, 9) in nuclear magnetic resonance imaging (MRI) and spectroscopy studies. Although these techniques have been used successfully to obtain valuable information about cerebral metabolism, they suffer from a number of limitations. There are potential risks associated with introduction of exogenous contrast agents, including anaphylaxis and radiation exposure. In addition, synthesis of the tracer compounds often involves considerable expense. The calculation of absolute values for perfusion in many of these techniques requires knowledge of the arterial input function, obtained by sequential arterial blood sampling. Despite these limitations, techniques employing exogenous contrast agents have been applied successfully in the study of cerebral blood flow. The development of a tracer technique which avoids these risks and limitations would represent a significant advance.

Recently, a quantitative and noninvasive MRI technique for perfusion imaging has been described which uses magnetically labeled arterial water as a freely diffusible endogenous tracer (10, 11). This technique has previously been used to measure perfusion in rat brain at the relatively high field strength of 4.7 T. Arterial water was labeled via either magnetic saturation (10) or inversion (11). Use of an inversion technique is preferable because the magnitude of the observed effect is larger. This method of perfusion measurement has been validated in rat brain (12) and in an isolated, perfused rat heart preparation (13). In this paper we describe our experience using this technique in human brain on a conventional 1.5-T commercial imaging system.

MATERIALS AND METHODS

Image Acquisition. All experiments were conducted on a 1.5-T imaging system (Signa, General Electric Medical Systems, Milwaukee). Human studies were performed with a protocol approved by the Institutional Review Board of the University of Pennsylvania. Informed consent was obtained from all volunteers.

Volunteers were asked to lie still with their eyes closed and were given ear plugs to reduce the noise of the gradient coils. Foam padding was used to limit head motion during the study. Lights in the magnet room were turned off. The static magnetic field shim was manually optimized and the proton water resonance was centered on resonance. A two-dimensional, refocused, gradient-echo pulse sequence was used to acquire inversion and control images. An off-resonance radio-frequency pulse was inserted in the interpulse interval which consisted of a series of 18.5-msec rectangular pulses separated by 1.6-msec gaps. An axial 5-mm-thick slice located ≈2 cm superior to the corpus callosum was imaged with a field of view of 24 cm, an echo time (TE) of 5 msec, and a repetition time (TR) of 100 msec. A fractional echo was used to minimize artifacts arising due to dephasing during readout and to minimize the sensitivity of the image to susceptibility effects (14). A homospoil y-gradient pulse of 4-msec duration and amplitude 1 G/cm was inserted between the end of the inversion pulse and the beginning of the observation pulse to attenuate residual transverse magnetization created by the inversion pulse. The image plane was placed at isocenter in the gradients prior to scanning.

The duration of the labeling pulse, T_{inv}, was 74 msec, corresponding to a 74% duty cycle. The amplitude of the labeling radio-frequency pulse varied between 23 and 33 mG (100–140 Hz). The specific absorption rate was estimated by extrapolating from the known specific absorption rate of the pulse sequence in the absence of the labeling pulse. Under these conditions the average specific absorption rate was below 0.4 W/kg. The amplitude of the inversion gradient was 0.5 G/cm. The offset frequency of the labeling pulse, ω_i, was chosen so that inversion occurred through a plane which approximately intersected the intracavernous portion of the internal carotid artery. The offset frequency varied between 6.3 and 10.6 kHz, corresponding to distances of 3–5 cm between the inversion and

The publication costs of this article were defrayed in part by page charge payment. This article must therefore be hereby marked "*advertisement*" in accordance with 18 U.S.C. §1734 solely to indicate this fact.

Abbreviations: MRI, magnetic resonance imaging; TE, echo time; TR, repetition time.

†To whom reprint requests should be addressed.

imaging planes. A quadrature birdcage transmit/receive head coil was used. For each slice, 64 phase-encodings were performed. Signal averaging was performed to achieve a signal/noise ratio greater than 150:1. This resulted in a typical acquisition time of 2–5 min. Inversion and control images were acquired by changing the sign of the offset frequency of the inversion irradiation.

A map of $T1_{app}$ was acquired by using a two-point inversion recovery measurement with TE = 12 msec and TR = 3000 msec. Images of the same slice were acquired with an inversion time, TI, of 1200 and 2400 msec. The apparent T1 was calculated by fitting the data to a monoexponential recovery curve. Acquisition of a $T1_{app}$ map required ≈8 min. The acquisition matrix for all images was 256 × 64. The total imaging time to obtain inversion, control, and $T1_{app}$ images was typically 12–18 min.

For respiratory rate studies, an inversion image was initially acquired while the subject breathed normally. The subject was then asked to hold his breath for 1 min while another inversion image was acquired. A total of four inversion images was acquired to increase the signal/noise ratio. After coming back to equilibrium, the subject was then asked to breath as rapidly and deeply as possible during acquisition of four more inversion images. Hypoventilation produces an increase in brain perfusion and hyperventilation produces a decrease in brain perfusion due to the regulation of cerebral blood flow by alterations in the arterial CO_2 concentration. Variations in the control image and the $T1_{app}$ image with changes in perfusion status are negligible.

Data Analysis. Perfusion maps were calculated according to Eq. **1**. Pixels containing only background noise were excluded by using a 10% threshold. The brain/blood partition coefficient, λ, was assumed to be constant at 0.90 ml/g (15). Based on cardiac-gated MRI measurements (16), the average velocity within the internal carotid artery was assumed to be 20 cm/sec, and the transit time, Δ, was assumed to be 200 msec for a 4-cm separation between the inversion and imaging planes. These values were used to estimate the effective degree of inversion.

Region-of-interest analysis of each perfusion map was performed by interactively selecting two regions ≈10 cm^2 in size each, one in each cerebral hemisphere. Values in these regions were automatically segmented into gray matter and white matter based on the $T1_{app}$. Any pixel with a $T1_{app}$ value between 0.9 and 1.1 sec was designated gray matter, and any pixel with $T1_{app}$ between 0.6 and 0.8 sec was designated white matter. Areas of high signal around bulk flow structures and at the periphery of the brain were avoided.

THEORY

Continuous inversion of the arterial water supplying the brain results in a small decrease in the steady-state image intensity. Specifically, perfusion, f, is given by

$$f = \frac{\lambda}{T1_{app}} \frac{(M_c - M_i)}{2\alpha' M_c}, \quad [1]$$

where M_i is the intensity in an image acquired with arterial inversion (inversion image), M_c is the intensity in an image acquired without arterial inversion (control image), λ is the brain/blood partition coefficient, and α' is the effective degree of arterial inversion (11). The quantity $T1_{app}$ is the apparent spin-lattice relaxation time, which is a function of the true T1 and perfusion, f (10):

$$\frac{1}{T1_{app}} = \frac{1}{T1} + \frac{f}{\lambda}. \quad [2]$$

The apparent T1 may be measured by a progressive saturation or inversion recovery experiment. The effective degree of arterial inversion, α', includes the effects of the duty cycle of the labeling pulse and of the transit time, Δ, for blood to pass from the site of inversion into the capillary beds (17) and is defined by

$$\alpha' = e^{-\Delta/T1_b}\left(\frac{T_{inv}}{TR}\right)\alpha, \quad [3]$$

where $T1_b$ is the spin-lattice relaxation time of arterial blood, T_{inv} is the duration of the inversion pulse, TR is the repetition time of the pulse sequence, and α is the degree of inversion defined by the labeling pulse at the site of inversion. Eq. **1** has been shown to be valid even under partially relaxed conditions (11).

We use the principle of transport-induced adiabatic fast passage (18–21) to continuously invert blood entering the brain. In this approach, constant low-amplitude irradiation is applied off-resonance in the presence of a magnetic field gradient. Spins which move through the gradient field undergo a frequency sweep by virtue of their motion. The component of spin velocity in the direction of the gradient (v), gradient strength (G_i), and irradiation amplitude, γB_i, define an adiabaticity factor, β, given by

$$\beta = \frac{(\gamma B_i)^2}{\gamma G_i v}. \quad [4]$$

The term in the denominator of Eq. **4** is the effective sweep rate of the pulse (units of radians/sec are assumed). The inversion efficiency, α, may be defined in terms of the initial z-magnetization (M_0) and the z-magnetization after passage through resonance (M_0') as

$$\alpha = \frac{(M_0 - M_0')}{2M_0}. \quad [5]$$

Highly efficient inversion will occur for a range of velocities given by the following inequality,

$$\frac{1}{T1_b}, \frac{1}{T2_b} << \frac{G_i v}{B_i} << \gamma B_i, \quad [6]$$

where $T1_b$ and $T2_b$ are the relaxation time constants of arterial blood. If the blood moves too slowly through the gradient, then relaxation effects dominate and inversion does not occur. If the blood moves too rapidly, the pulse becomes nonadiabatic and inversion does not occur.

RESULTS

The T1 of anticoagulated whole blood was determined to be 1.4 sec based on a multiple-point inversion–recovery measurement. Computed spin simulations and measurements in experimental flow phantoms were performed to determine the dependence of the inversion efficiency, α, on the adiabaticity factor, β (21). For the choice of parameters defined by our experiment (v = 20 cm/sec, γB_i = 140 Hz, and G = 0.5 G/cm), the adiabaticity factor, β, is ≈2.9, which corresponds to 98% efficient inversion. This result, combined with a duty cycle of 0.74 and the estimated transit time of 200 msec, yields an effective degree of inversion, α', of 0.63. To visualize the effect of the irradiation on blood flow in the ICA, cardiac-gated images were acquired with the same parameters given above but with the inversion gradient in the frequency-encoding direction (Fig. 1). The instantaneous velocity, calculated from band displacement, never fell below

10 cm/sec, and inversion was observed during every phase of the cardiac cycle.

As we use a single coil to apply the inversion and observation pulses, the off-resonance effects of the inversion pulse represent a potential source of error in the measurement (21). The labeling pulse affects magnetization in the image plane directly or via cross-relaxation phenomena (22, 23). Images were acquired to determine the degree of saturation due to the inversion pulse as a function of the frequency offset for the choice of pulse parameters used in the perfusion experiments. The results appear in Fig. 2, in which we have also indicated the frequency range occupied by a 5-mm-thick slice in an inversion gradient of 0.5 G/cm for a typical choice of frequency offset. The graph illustrates that the labeling pulse results in significant saturation of spins in the image plane. As previously described (11), an adequate control image must balance this effect, which may be accomplished by changing the sign of the offset frequency of the labeling pulse. The graph also demonstrates that there is relatively little variation of the off-resonance effects across the slice thickness. This implies that errors due to asymmetry in spin density and relaxation characteristics across the slice should be negligible (21).

Images of $T1_{app}$ and perfusion of a normal volunteer appear in Fig. 3 *A* and *B*, respectively. Inversion of arterial water was observed to result in a decrease in signal intensity in all parts of the brain. Included in the image is a piece of bovine muscle tissue, which is known to experience relatively large cross-relaxation effects (22). Negligible residual signal is obtained from the nonperfused muscle tissue. Although there is rough correlation with the gray matter/white matter distribution in the $T1_{app}$ image, significant nonrandom local variations are present in the perfusion image. Some regions of artifactually

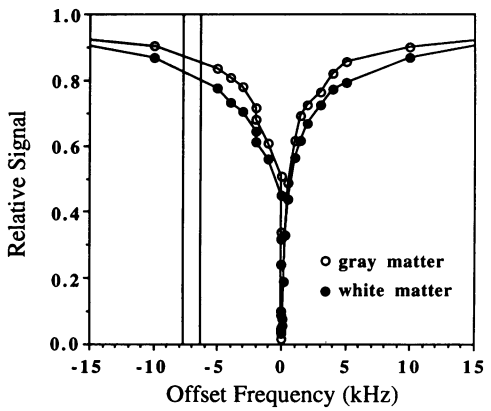

FIG. 2. Off-resonance effects of the labeling pulse under conditions similar to those used in the perfusion imaging experiments. The normalized image intensity is plotted as a function of the offset frequency of the labeling pulse for gray matter (○) and white matter (●). The labeling pulse amplitude, γB_1, was 100 Hz and the duty cycle was 74%. Off-resonance effects are slightly more significant in white matter. The frequency range occupied by a 5-mm-thick slice is indicated by solid vertical lines. It is centered on a typical frequency offset used in the perfusion imaging experiments.

high signal intensity are present which probably represent errors due to either chemical shift (fat in the scalp), bulk flow (midline vessels), or asymmetry effects (at the periphery of the brain). Results of perfusion measurements in a set of nine normal volunteers appear in Table 1. The ratio of perfusion between gray matter and white matter is ≈2.3, in general agreement with the literature (24). To illustrate the errors which can arise due to off-resonance effects, a perfusion map

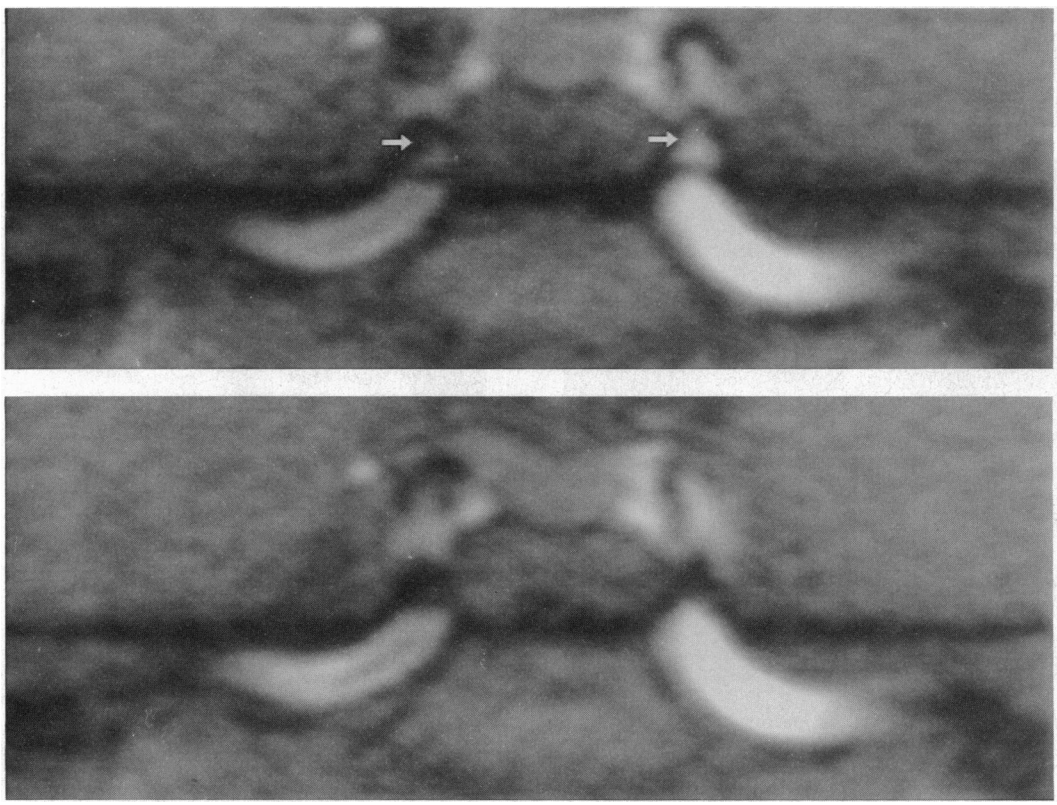

FIG. 1. Inversion of arterial blood in the intracavernous portion of the internal carotid artery. Gated coronal images were acquired in the presence of inversion irradiation, γB_1, of 70 Hz (*Lower*) or 140 Hz (*Upper*) and in an inversion gradient of 0.5 G/cm in the frequency-encoding (vertical) direction under otherwise identical conditions. The plane of inversion is indicated by the horizontal saturation band, which lies approximately at the level of the hypothalamus. The weaker radio frequency results in spin saturation, whereas the stronger radio frequency results in the development of an inversion band (arrows) in arterial blood.

was obtained from another individual under the same conditions except that the slice thickness was 15 mm (Fig. 4). The halo of bright signal surrounding the brain is the result of significant spin distribution asymmetry which occurs in this region, leading to failure to control for off-resonance effects.

The effect of respiratory status was studied in a set of three normal volunteers. The average global perfusion rate (ml·100 g^{-1}·min^{-1}) was 34 ± 16 during hyperventilation, 66 ± 9 at rest, and 84 ± 8 during breath holding. Perfusion differed significantly in each of the three respiratory states ($P < 0.05$, Student t test). As expected, cerebral perfusion increased during hypoventilation and decreased during hyperventilation (25). Changes in control images as a function of respiratory rate were observed to be below the level of the noise.

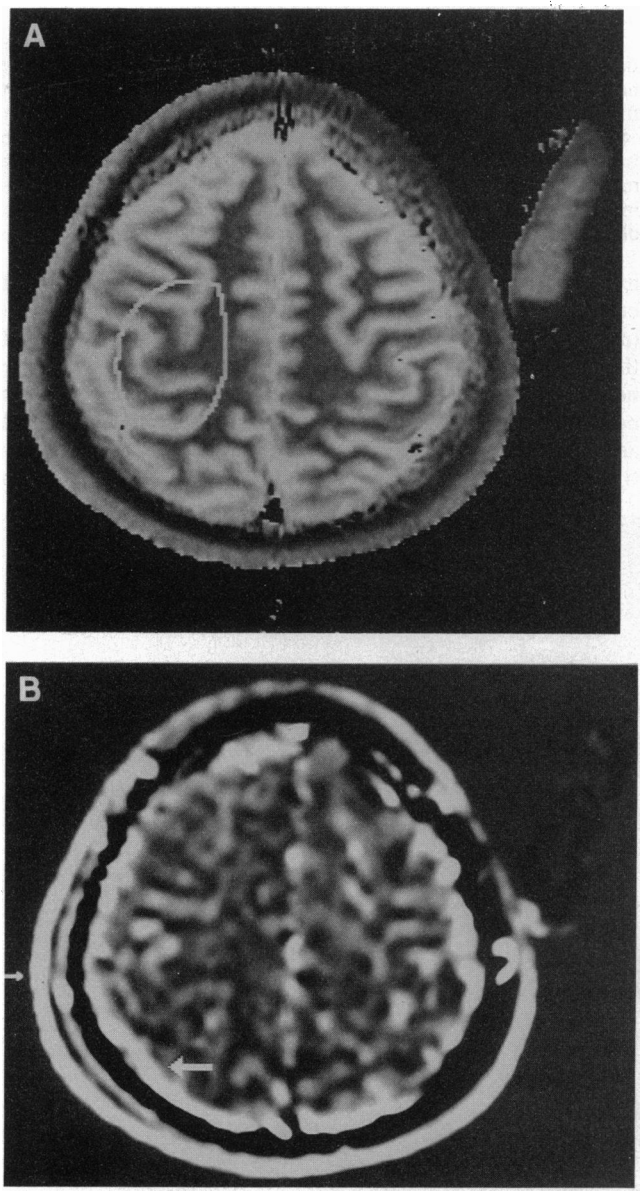

FIG. 3. Images of the T1app (*A*) and perfusion (*B*) of a normal resting volunteer. T1app values are scaled between 0 and 1.5 sec, and perfusion values are scaled between −100 and 250 ml·100 g^{-1}·min^{-1}. A nonperfused piece of bovine muscle tissue appears in the T1app image but not in the perfusion image. The perfusion image contains artifacts arising from chemical shift effects (small arrow) and spin asymmetry (large arrow). A typical region of interest used in the data analysis is indicated on the T1app map. A uniformly weighted local average and median filter was applied to reduce noise in the perfusion image.

Table 1. Average perfusion rates in a set of nine volunteers determined by region-of-interest analysis

Subject	Perfusion, ml·100 g^{-1}·min^{-1}		
	Gray matter	White matter	Whole brain
1	86	39	48
2	120	38	61
3	97	25	46
4	78	33	49
5	84	49	58
6	110	31	49
7	77	38	39
8	99	49	66
9	85	43	48
Total	93 ± 16	38 ± 10	52 ± 8

DISCUSSION

These results demonstrate that quantitative images of perfusion can be obtained from human brain at 1.5 T with a commercial imaging system. The advantages of this technique are that it is noninvasive; does not require exogenous tracers, arterial blood sampling, or ionizing radiation; and allows for measurement of absolute values for cerebral perfusion. As the effects on image intensity obtained by arterial inversion are extremely small at 1.5 T, potential sources of error must be carefully minimized. In addition, because this is a steady-state technique, acquisition of inversion and control images cannot be interleaved. This necessitates very good temporal stability in the imaging equipment as well as careful restriction of patient motion. Improvement in signal/noise ratio for the perfusion effect may be obtained by using fast imaging methods to reduce data acquisition time (26) or by performing the experiment at a higher static-field strength. As the T1 of arterial blood is significantly longer at 4.7 T (11), one may obtain a higher effective degree of inversion and increase the perfusion effect. Additional improvement may be obtained by using separate coils for arterial inversion and image acquisition, as this will eliminate

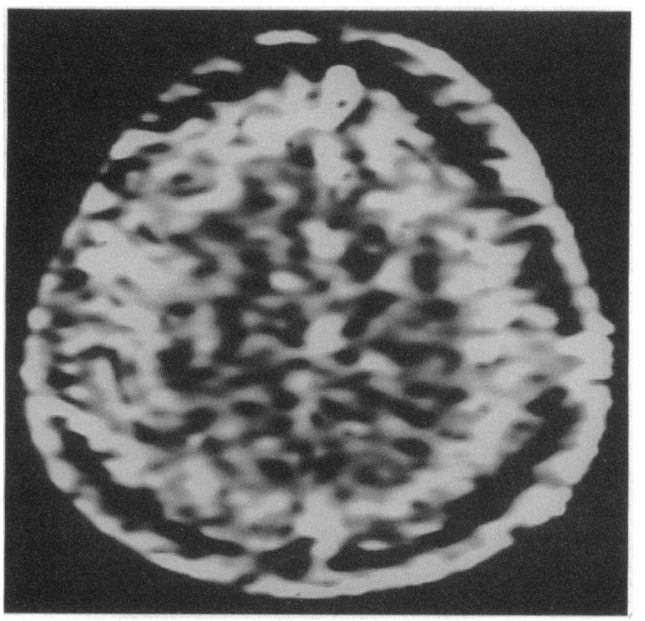

FIG. 4. Perfusion image of a normal resting volunteer, acquired under conditions identical to those of Fig. 3 except that the slice thickness was 15 mm. A bright halo appears at the periphery of the brain due to failure to control for off-resonance effects at the larger slice thickness.

the considerable signal loss due to cross relaxation. This allows for three-dimensional or multislice imaging in the abscence of off-resonance effects and offers the additional advantage that the perfusion distribution of individual arteries can be measured.

The values for perfusion are dependent on the values assumed for the transit time and the inversion efficiency. Noninvasive techniques have been developed, however, which allow for direct measurement of these important parameters (17, 27). Application of these techniques to studies of human brain would eliminate a potential source of error.

Artifacts due to bulk flow appear in the perfusion images. These may be attenuated by using balanced bipolar gradient pulses which dephase flowing spins (11). We found, however, that incorporation of such pulses in our imaging sequence extended TE and resulted in an unacceptable loss of signal/noise ratio.

The successful measurement of brain perfusion using this approach will enhance the diagnostic capabilities of MRI for neurological disease. Because the risks of this technique are essentially those of routine MR imaging, one may perform repeated studies of the same individual and more easily perform perfusion studies in children. In addition, regional changes in brain perfusion may be used to map the cortical localization of sensory responses (5, 28, 29) and higher cognitive function. The increased spatial resolution of MRI, the automatic registration of perfusion images with highly detailed anatomical images, and the ability to conduct an integrated, multinuclear examination represent important advantages of magnetic resonance perfusion imaging over existing methods for studies in human brain.

We thank Drs. Mitchell Schnall, Robert Lenkinski, and Ruben Gur for valuable discussion and technical advice. We acknowledge the excellent technical assistance of Larry Dougherty and Norman Butler. This work was supported by National Institutes of Health Grants RR02305 and GL07614. The first author is Medical Scientist Training Program Fellow supported by National Institutes of Health Grant GM07170 and by a grant from the University Scholars Council of the University of Pennsylvania.

1. Ter-Pogossian, M. M., Eichling, J. O., Davis, D. O., Welch, M. J. & Metzger, J. M. (1969) *Radiology* **93,** 31–40.
2. Herscovitch, P., Markham, J. & Raichle, M. E. (1983) *J. Nucl. Med.* **24,** 782–789.
3. Gur, D., Good, W., Wolfson, S. K., Yonas, H. & Shabason, L. (1982) *Science* **215,** 1267–1268.
4. Rosen, B. R., Belliveau, J. W., Vevea, J. M. & Brady, T. J. (1990) *Magn. Reson. Med.* **14,** 249–265.
5. Belliveau, J. W., Kennedy, D. N., McKinstry, R. C., Buchbinder, B. R., Weisskoff, R. M., Cohen, M. S., Vevea, J. M., Brady, T. J. & Rosen, B. R. (1991) *Science* **254,** 716–719.
6. Ackerman, J. J. H., Ewy, C. S., Becker, N. N. & Shalowitz, R. A. (1987) *Proc. Natl. Acad. Sci. USA* **84,** 4099–4104.
7. Detre, J. A., Subramanian, V. H., Mitchell, M. D., Smith, D. S., Kobayashi, A., Zaman, A. & Leigh, J. S. (1990) *Magn. Reson. Med.* **14,** 389–395.
8. Eleff, S. M., Schall, M. D., Laszlo, L., Osbakken, M., Subramanian, V. H., Chance, B. & Leigh, J. S. (1988) *Magn. Reson. Med.* **7,** 412–424.
9. Detre, J. A., Eskey, C. J. & Koretsky, A. P. (1990) *Magn. Reson. Med.* **15,** 45–57.
10. Detre, J. A., Leigh, J. S., Williams, D. S. & Koretsky, A. P. (1991) *Magn. Reson. Med.* **22,** 1–9.
11. Williams, D. S., Detre, J. A., Leigh, J. S. & Koretsky, A. P. (1992) *Proc. Natl. Acad. Sci. USA* **89,** 212–216.
12. Walsh, E. G., Minematsu, K., Leppo, J., Gilmore, M. P., Adzamil, K. & Moore, S. C. (1992) *Book of Abstracts: Eleventh Annual Meeting of the Society of Magnetic Resonance in Medicine* (Soc. Magn. Reson. Med., Berkeley, CA), p. 1140.
13. Grandis, D. J., Williams, D. S., Zhang, W. & Koretsky, A. P. (1992) *Book of Abstracts: Eleventh Annual Meeting of the Society of Magnetic Resonance in Medicine* (Soc. Magn. Reson. Med., Berkeley, CA), p. 2413.
14. Ogawa, S., Lee, T. M., Nayak, A. S. & Glynn, P. (1990) *Magn. Reson. Med.* **14,** 68–78.
15. Herscovitch, P. & Raichle, M. E. (1985) *J. Cereb. Blood Flow Metab.* **5,** 65–70.
16. Firmin, D. N., Klipstein, R. H., Hounsfield, G. L., Paley, M. P. & Longmore, D. B. (1989) *Magn. Reson. Med.* **12,** 316–322.
17. Zhang, W., Williams, D. S., Detre, J. A. & Koretsky, A. P. (1992) *Magn. Reson. Med.* **25,** 362–371.
18. Abragam, A. (1961) *The Principles of Nuclear Magnetism* (Oxford Univ. Press, Oxford), p. 65.
19. Dixon, W. T., Du, L. N., Faul, D. D., Gado, M. & Rossnick, S. (1986) *Magn. Reson. Med.* **3,** 454–462.
20. Lee, H. K., Nalcioglu, O. & Moran, P. R. (1991) *Magn. Reson. Imag.* **9,** 115–127.
21. Roberts, D. A., Bolinger, L., Detre, J. A., Insko, E. K., Bergey, P. & Leigh, J. S. (1993) *Magn. Reson. Med.* **29,** 631–636.
22. Wolff, S. D. & Balaban, R. S. (1989) *Magn. Reson. Med.* **10,** 135–144.
23. Grad, J. & Bryant, R. G. (1990) *J. Magn. Reson.* **90,** 1–10.
24. Mazziotta, J. C. & Phelps, M. E. (1986) in *Positron Emission Tomography and Autoradiography: Principles and Applications*, eds. Phelps, M., Mazziotta, J. & Schelbert, H. (Raven, New York), p. 499.
25. Hurwitz, K., Ashwal, S., Tomasi, L., Schneider, S. & Thompson, J. (1992) in *Cerebral Blood Flow Measurement with Stable Xenon-Enhanced Computed Tomography*, ed. Yonas, H. (Raven, New York), pp. 140–148.
26. Mansfield, P. & Maudsley, A. A. (1977) *Br. J. Radiol.* **50,** 188–192.
27. Zhang, W., Williams, D. S. & Koretsky, A. P. (1993) *Magn. Reson. Med.* **29,** 416–421.
28. Kwong, K. K., Belliveau, J. W., Chesler, D. A., Goldberg, I. E., Weisskoff, R. M., Poncelet, B. P., Kennedy, D. N., Hoppel, B. E., Cohen, M. S., Turner, R., Cheng, H.-M., Brady, T. J. & Rosen, B. R. (1992) *Proc. Natl. Acad. Sci. USA* **89,** 5675–5679.
29. Frahm, J., Klaus-Dietmar, M. & Hanicke, W. (1993) *Magn. Reson. Med.* **29,** 139–144.